Strength of Flexible Composites: Effect of Fiber Scaling

N.M. Hossain[1]
Eastern Washington University, Cheney, WA-99004, USA

W.M. Peterson[2]
Montana State University, Bozeman, MT-59717, USA

K. Woo[3]
Chungbuk National University, Cheongju, Chungbuk 361-763, Republic of Korea

and

C. H. Jenkins[4]
Montana State University, Bozeman, MT-59717, USA

This paper represents a continued research to pursue the possible advantages of utilizing nanofibers instead of conventional fibers in flexible composite materials. An advantage of using nanofibers is to increase the fiber surface area, while the fiber volume fraction remains the same. Reducing fiber diameter has the promise of providing composites whose strength is equivalent to those with conventional fibers but at reduced weight and increased flexibility. In this research, several unit cell models were analyzed under tensile and bending loads where the surface area of fiber was increased gradually using the reduced fiber diameter. For each unit cell model and loading situation, the axial and shear stresses developed in the fiber region were studied. In both tensile and bending loads, unit cell models with reduced fiber diameter were found to offer shorter ineffective fiber lengths. The ineffective fiber length represents the length of fiber required for complete load redistribution from matrix to fiber, and also the region where the fiber stress is not yet fully developed. In addition, as the fiber surface area increases with a reduction in fiber diameter, the unit cell models with reduced fiber diameter were also found to offer reduced shear stress both in tensile and bending simulations. Therefore, if the composite strength depends on fiber surface area, then a composite consisting of fibers with reduced diameter will be stronger than a conventional composite prepared with same volume fraction or conversely will be lighter at the same strength.

Nomenclature

a, b	=	side dimension of unit cell
A_s	=	surface area of fiber
A_x	=	cross sectional area of fiber
d	=	fiber diameter
D	=	depth of unit cell
H	=	half width of unit cell
M_x	=	bending moment about x-axis
N	=	number of fibers in a unit cell
L	=	length of unit cell
RVE	=	Representative Volume Element
R_z	=	reaction force (absolute value) along z-axis under bending load
u	=	displacement
V_f	=	fiber volume fraction
W	=	width of unit cell

[1] Assistant Professor, Department of Engineering and Design, Member AIAA, Email: nhossain@ewu.edu.
[2] Graduate Student, Department of Mechanical and Industrial Engineering, Member AIAA.
[3] Professor, Department of Structural System and CAE. Member AIAA.
[4] Professor and Head, Department of Mechanical and Industrial Engineering. Associate Fellow AIAA.

σ = axial stress in fiber
τ = shear stress at fiber/matrix interface

I. Introduction

THE advancement of all space missions is significantly influenced by the development of engineering materials with unique mechanical and physical properties. One of the goals of all gossamer spacecraft is to reduce the structural weight, and in so doing, to minimize launch cost. One way to achieve this objective is through the replacement of metallic structures with advanced composites. Currently, composite materials are widely used in many engineering applications because of their light weight, multifunctional properties and low cost. Composites are engineered materials made from two or more constituents with significantly different physical or chemical properties, and which remain separate and distinct on a microscopic level within the finished structure. A composite material typically consists of relatively strong and stiff fibers in a tough resin matrix. Fig. 1 represents a simplified concept of a unidirectional composite materials with fiber and matrix, showing the Representative Volume Element (RVE) – the smallest cell (as denoted by the dotted line) to describe the individual composite constituents.

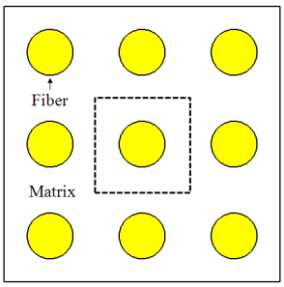

Figure 1. Simplified concept of composite materials and the Representative Volume Element (RVE).

In a series of papers by Aboudi,[1,2] the overall behavior of composite materials was explored through micromechanical analysis. The analysis was performed using an RVE approach to predict the elastic, thermoplastic, viscoelastic and viscoplastic responses of composites. Goh et al.[3] compared different solutions for shear-lag models for describing the stress transfer from an elastic matrix to a fiber in a composite material. Chon et al.[4] developed an analytical solution for predicting the axial and interfacial shear stress distributions along a single fiber of a randomly oriented chopped-fiber composite. Xia et al.[5] compared the shear-lag theory with finite element models for stress transfer in a fiber-reinforced composite. The stress transfer from broken to unbroken fibers is studied using a detailed 3D finite element model and then compared with standard shear-lag model. Milliren[6] developed several numerical models using ABAQUS/CAE, and compared the stress distribution with standard shear-lag theories. These models were capable of utilizing interphase if desired, and was capable of off-axis loading scenarios. Hossain et al.[7] studied the effect of fiber diameter on composite strength by developing several unit cell models with reduced fiber diameter while keeping the fiber volume fraction the same.

The purpose of the current work was to investigate the effects of fiber diameter and other parameters on composite strength. Reducing fiber diameter has the promise of providing composites whose strength is equivalent to those with conventional fiber diameters but at reduced weight and increased flexibility. Moreover, reduced fiber diameters may be the only option when trying to reinforce thin membranes whose thickness is already less than conventional fiber diameters.

Finite element (FE) analyses were performed to explore the effect of a fiber scaling that increases the surface area of fiber, to pursue the possible advantages in composite strength. Additional numerical analyses were conducted to examine how the composite strength would be affected by changing the fiber volume fraction, and moduli ratio of fiber and matrix materials. Mechanical properties of compliant fiber and matrix materials, applicable to gossamer spacecrafts, were used in the numerical analyses.

An advantage of reducing the fiber diameter is to increase the fiber surface area, which, e.g., can help to compensate for imperfect fiber-matrix bonding during failure situation. It can be easily shown that the composite with reduced fiber diameter contains significantly more fiber surface area compared to the conventional composite at the same volume fraction. Fig. 2 illustrates the concept of maintaining the same fiber cross-sectional area while increasing fiber surface area.

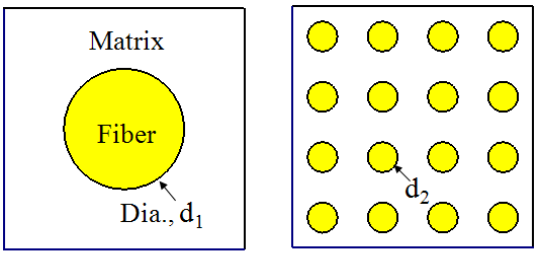

Figure 2. Illustration of using nanofibers, where $d_1/d_2 = 4$, to increase the fiber surface area with constant volume fraction.

In Table 1, which relates to Fig. 2, both conventional and reduced fiber (i.e., fiber with reduced diameter) models have the same fiber cross sectional area (A_x). Therefore, assuming a unit depth both models have same fiber volume fraction (V_f). Note that, the fiber surface area (A_s) in the reduced fiber model has been increased by 4 times compared to the conventional model. Subscripts c and r, used in Table 1, represents the conventional and reduced fiber composite models, respectively. In general, it will be seen that the surface area of fibers in reduced fiber composite will be higher than that of the conventional composite by a factor of $\sqrt{N}$, where N represents the total number of reduced fibers that replace the conventional fibers at constant fiber volume fraction. Therefore, if the composite strength depends on fiber surface area, then a composite consisting of fiber with reduced diameter will be stronger than a conventional composite prepared with same volume fraction, or conversely will be lighter at the same strength. However, the effects of down-scaling the fiber diameter on composite strength is almost unrevealed.

Table 1: Comparing cross-sectional (A_x) and surface (A_s) area between conventional and reduced fiber composite models

(a) Conventional Composite	(b) Reduced Fiber Composite
$(A_x)_c = (\pi/4)(d_1)^2$	$(A_x)_r = 16*(\pi/4)(d_2)^2$ $= 16*(\pi/4)(d_1/4)^2$ $= (\pi/4)(d_1)^2$
$(A_s)_c = (\pi)(d_1)$	$(A_s)_r = 16*(\pi)(d_2)$ $= 16*(\pi)(d_1/4)$ $= 4*(\pi)(d_1) = 4*(A_s)_c$

II. Procedure and Numerical Model

The strength of composites was investigated by analyzing several *unit cell* models maintaining the same fiber volume fraction, but with increased surface area of fiber. A unit cell represents the smallest building block, whose exact repetition in three-dimensional pattern could generate the whole structure. For example, Fig. 3(a) represents a *unit cell* of conventional composite, named UC-1, with equal side dimension a and fiber diameter d_1. Similarly, Fig. 3(b) represents another unit cell, named UC-2, with equal side dimension b and reduced fiber diameter d_2, where $d_2 < d_1$. Here, both the upper and lower boundaries are free surfaces and the structures repeat only in the horizontal direction, not in the thickness direction. This makes the unit cell in Fig. 3(a) 1-fiber model through the thickness, and the one in Fig. 3(b) 2-fiber model. Both unit cells have the same fiber volume fraction, V_f. Therefore, assuming unit depth

$$\frac{\frac{\pi}{4} * d_1^2}{a^2} = \frac{\frac{\pi}{4} * d_2^2}{b^2} \qquad (1)$$
$$\Rightarrow \frac{b}{a} = \frac{d_2}{d_1}$$

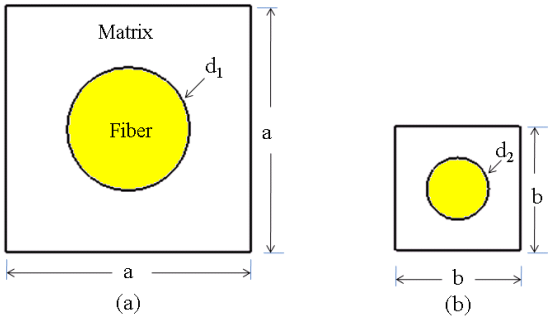

Figure 3. Illustration of unit cell concept maintaining same fiber volume fraction.

Both unit cell models will also have same amount of fiber, i.e., the same total fiber cross-sectional area A_f. Therefore,

$$N*\left(A_f\right)_{UC-2} = \left(A_f\right)_{UC-1}$$
$$\Rightarrow N = \left(\frac{d_1}{d_2}\right)^2 \tag{2}$$

where N represents number of fibers with reduced diameter. For example, if $d_2 = 0.5* d_1$, then from Eqn. 2, $N = 4$ (Fig. 4). The ratio of fiber surface area may be shown to be $(A_s)_{uc\text{-}2}/(A_s)_{uc\text{-}1} = 4\pi d_2/\pi d_1 = 2$. Then UC-2 has twice the surface area of fiber compared to UC-1, while maintaining same V_f and A_f.

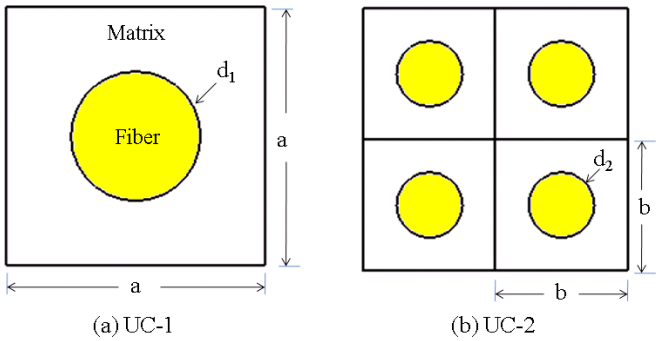

Figure 4. Illustration of unit cell concept with increased surface area (A_s) while maintaining same fiber volume fraction (V_f) and cross sectional area (A_f).

III. Results and Discussions

The numerical analysis of all unit cell models was performed using the finite element code ANSYS. Unit cell models were used for tensile and bending simulations. The quarter symmetric model of UC-1 with geometric dimensions, boundary conditions, and a 3D view is shown in Fig. 5. The length (L) of the unit cell model was kept to 5*D, where D represents the fiber diameter. The analysis was performed assuming that the fiber was broken within the matrix as depicted in Fig. 5(c). Therefore, boundary displacement loading was assigned only to matrix at the front surface (z = L). Similar boundary conditions and loading were applied to the other unit cell models. The numerical model is assumed to be infinitely repeated in the global x- directions. Therefore, a repeating boundary condition (RBC) was applied to the right edge, which ensures the same x-displacement (u_1) at x = 5. The entire back surface (z = 0) was constrained in its normal direction (z).

The displacement equations to enforce the required boundary conditions for tensile simulation are mentioned below, where u_1, u_2, and u_3 represent the x, y, and z- displacement, respectively:

Symmetry boundary conditions are applied to the left and bottom surfaces:

1) $u_1(0,y,z) = 0$,
2) $u_2(x,0,z) = 0$,

The rear surface at $z = 0$ is constrained in the z-direction:

3) $u_3(x,y,0) = 0$,

Repeating boundary condition (RBC) is applied to the right surface:

4) $u_1(5,y,z) = \delta_1$,

Notice that the RBC is such that all nodes on the right surface displace the same amount in the x-direction. Finally, a boundary displacement is applied only to the matrix nodes located at the front surface:

5) $u_3(x,y,L) = \delta_3$

The material properties are linear elastic and include Young's modulus (E) and Poisson's ratio (ν). Numerical analyses were conducted using the mechanical properties of lightweight fiber and matrix materials. In this research, standard values of Vectran (E = 75 GPa = $75x10^{-3}$ N/μm^2, ν = 0.3) and Polyethylene (E = 0.69 GPa = $0.69x10^{-3}$ N/μm^2, ν = 0.3) were used to mimic the fiber and matrix materials, respectively.

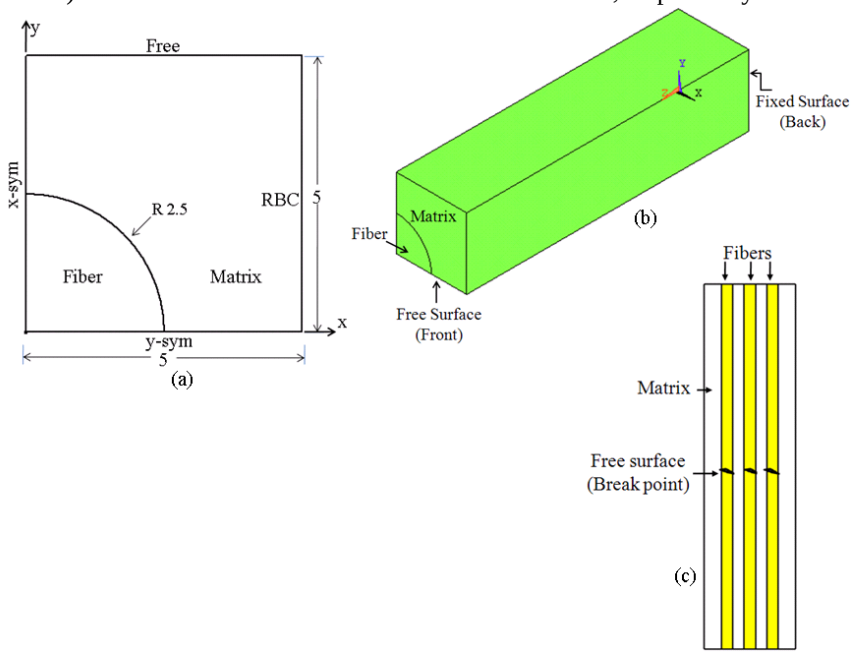

Figure 5. Quarter symmetric numerical model of UC-1 displaying geometric dimension (in micron) and boundary conditions.

The axial and shear stresses developed in the fiber material were compared between the unit cell models. Axial stress was recorded at the fiber center (at x = 0, y = 0 and z = 0 to L) and fiber-matrix interface (at x = fiber radius, θ = 90 degree and z = 0 to L), where the shear stress was recorded only at the fiber-matrix interface. The nodal location where the axial and shear stress data are recorded is shown in Fig. 6.

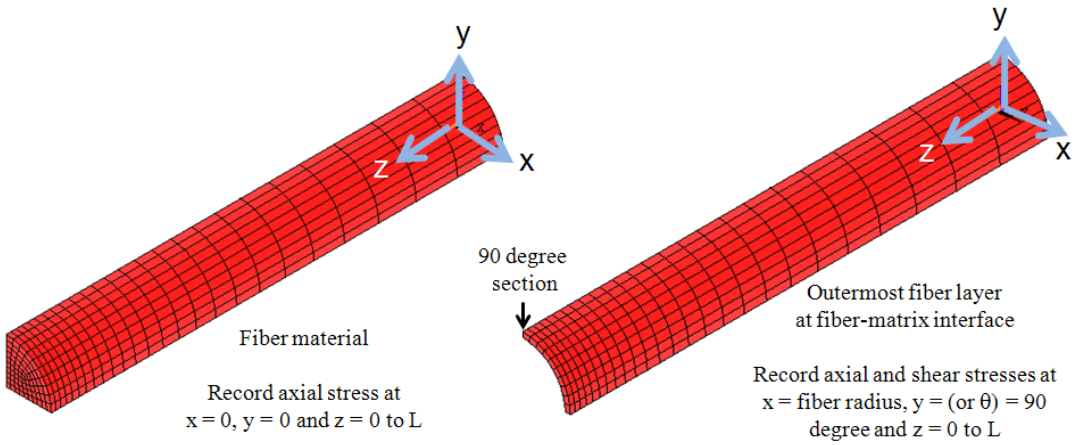

Figure 6. Nodal locations where the axial and shear stresses data are recorded.

The stress distribution along the fiber center and the fiber-matrix interface for an arbitrary boundary displacement is shown in Fig. 7. The stress distribution pattern was found to be different at the two different regions. Axial stress was found to be the maximum near the free end at the fiber-matrix interface, and gradually decreases towards the fixed end. The magnitude of the axial stress at the fiber center and fiber-matrix interface became coincident at non-dimensional length z'/D = 0.8, where z' = L-z. Note, z'= 0 at the free end (z = L) and z'= L at the fixed end (z = 0).

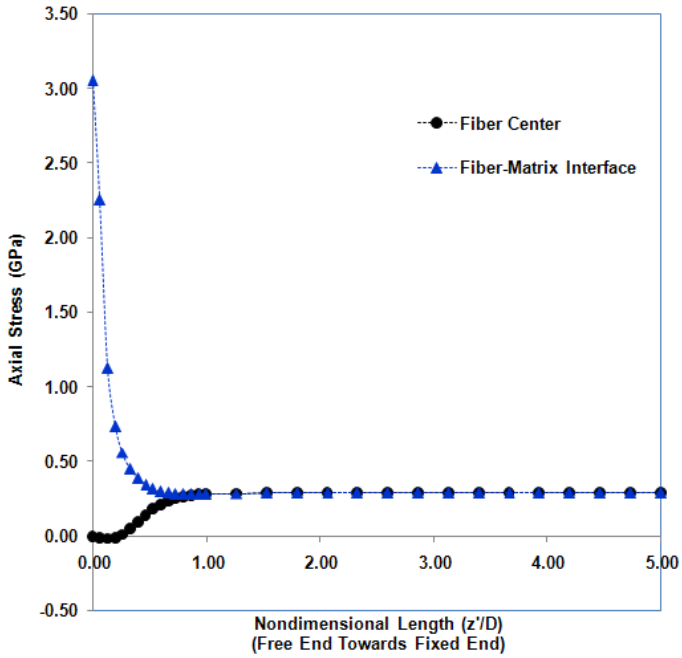

Figure 7. Axial stress distributions along the fiber center and fiber-matrix interface.

As boundary displacement load was applied in tensile simulation, reaction forces were developed at the back fixed surface. For a fair comparison between the unit cell models, the boundary displacement applied to unit cell models was tuned to get the same reaction force at the back fixed surface. The axial stress distribution pattern was found to be the same with changing the boundary displacement loading.

The axial and shear stresses developed in the fiber region were then compared between the UC-1 and UC-2 models, as shown in Fig. 4 before. The axial stress distribution along the fiber center and fiber-matrix interface is

shown in Fig. 8. The axial stress developed at the fiber-matrix interface and near the free end of UC-2 was found to be distinctly reduced compared to the UC-1, as shown in Fig. 8 (b).

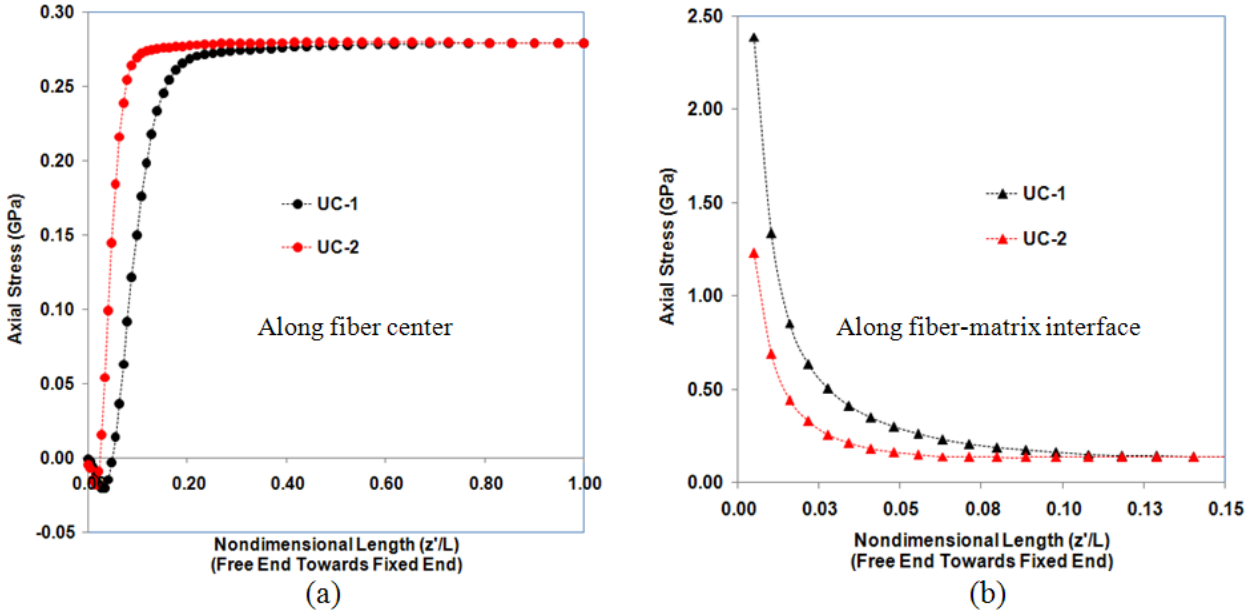

Figure 8. Axial stress distribution for UC-1 and UC-2, (a) along fiber center, (b) along fiber-matrix interface.

The unit cell models were also analyzed to check how the *ineffective fiber length* would differ with reducing the fiber diameter. In the context of the current problem, the ineffective fiber length is defined to be the length that carries less than 90% of the maximum fiber stress. Fig. 9 clearly indicates that the UC-2 with reduced fiber diameter has shorter fiber ineffective length compared to the UC-1. Therefore, stress (or load) will be transferred more quickly from matrix to fiber in UC-2 with reduced fiber diameter compared to UC-1.

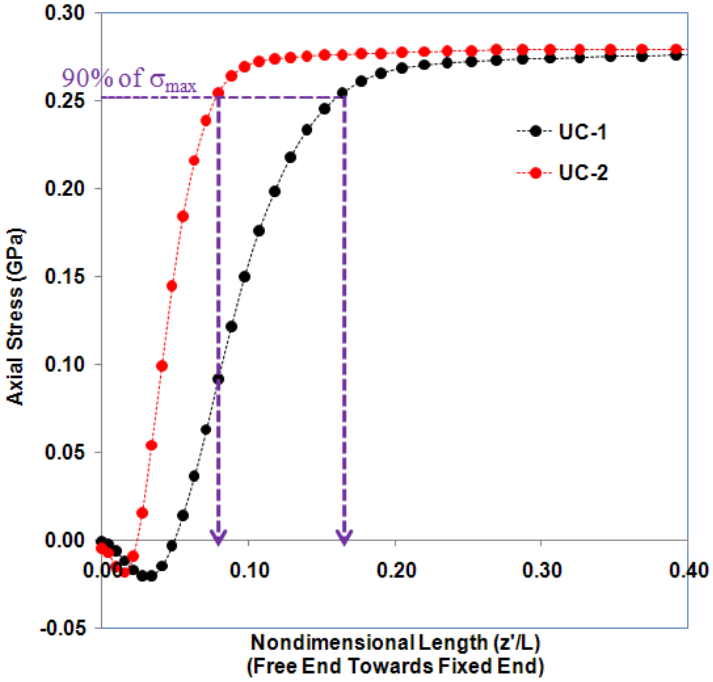

Figure 9. Comparison of ineffective fiber length for UC-1 and UC-2.

Shear stress was found to be the maximum near the free end and gradually decreased towards the fixed end. Fig. 10 represents the shear stress distribution at the fiber-matrix interface for UC-1 and UC-2. Stress was plotted separately for different regions to minimize the difference in scaling effect. In UC-2, the surface area of fiber was increased by 100% compared to UC-1. Therefore, the shear stress in UC-2 was found significantly reduced compared to the UC-1.

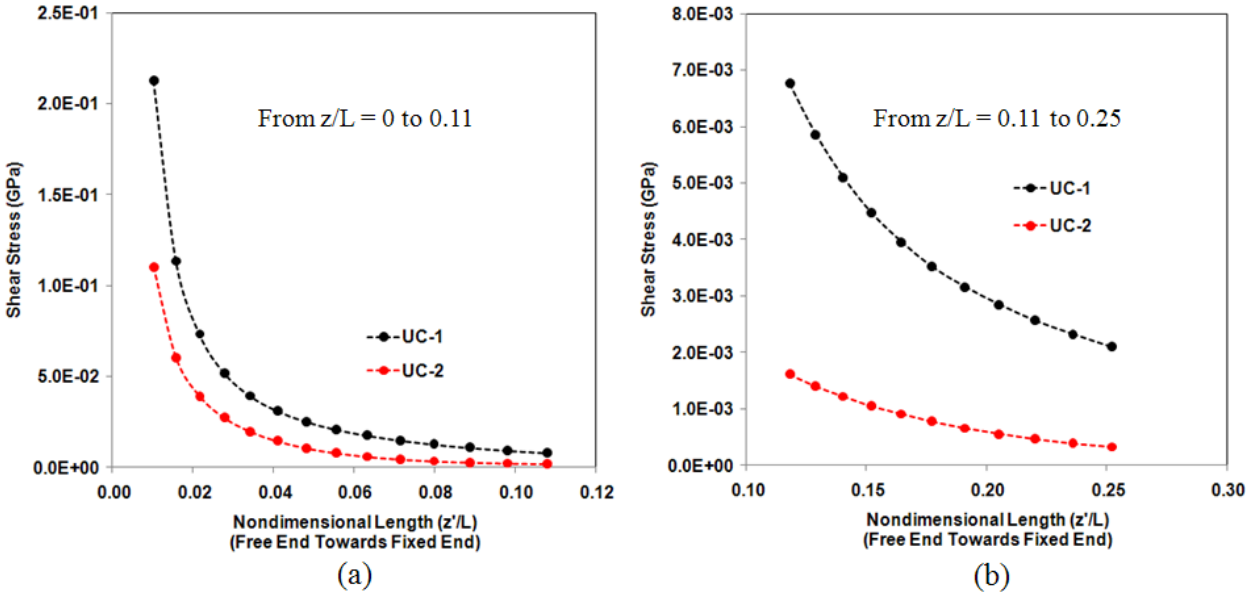

Figure 10. Shear stress distribution for UC-1 and UC-2 for nondimensional length, (a) z'/L = 0 to 0.11, (b) z'/L = 0.11 to 0.25

The UC-1 model was analyzed again for different parametric studies. For each case, the boundary displacement assigned to matrix nodes was tuned to get the same reaction force at the back fixed wall. First, the effect of fiber volume fraction was examined. The axial stress was found to be reduced in proportion by increasing the fiber volume fraction as expected, and shown in Fig. 11. Similar result was obtained for shear stress distribution as shown in Fig. 12. The axial stress distribution along the fiber center was also analyzed to check the ineffective fiber length. In this case, the local axial stress was normalized by the corresponding maximum stress. It was found that composite model with the minimum fiber volume fraction offered the shortest ineffective fiber length, that is, the load was transferred from matrix to fiber within the shortest distance, as shown in Fig. 13.

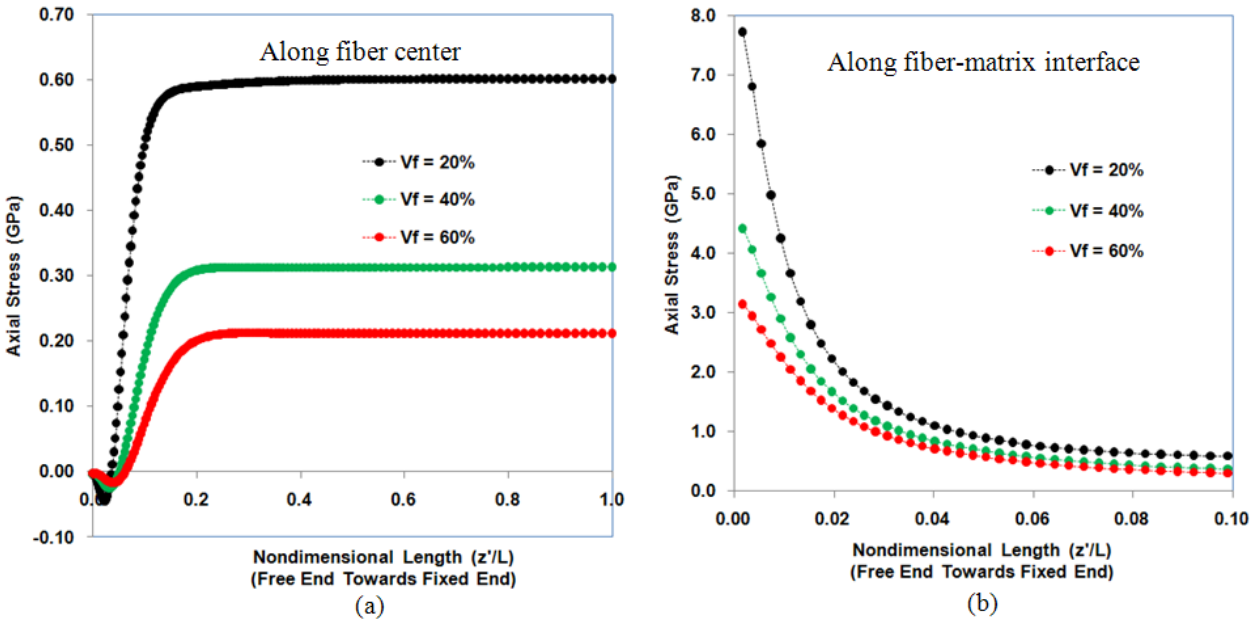

Figure 11. Axial stress distribution with changing fiber volume fraction, (a) along fiber center, (b) along fiber-matrix interface.

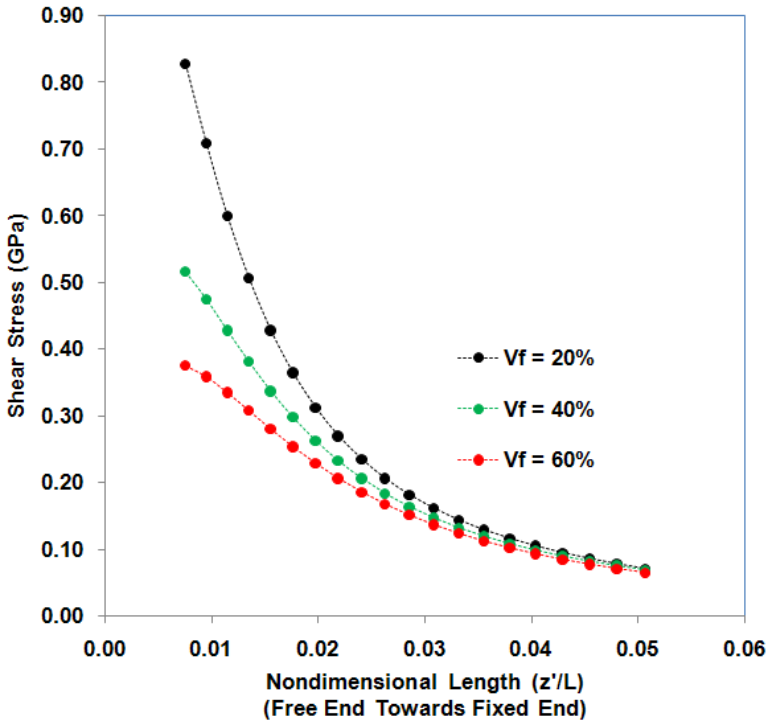

Figure 12. Shear stress distribution with changing fiber volume fraction.

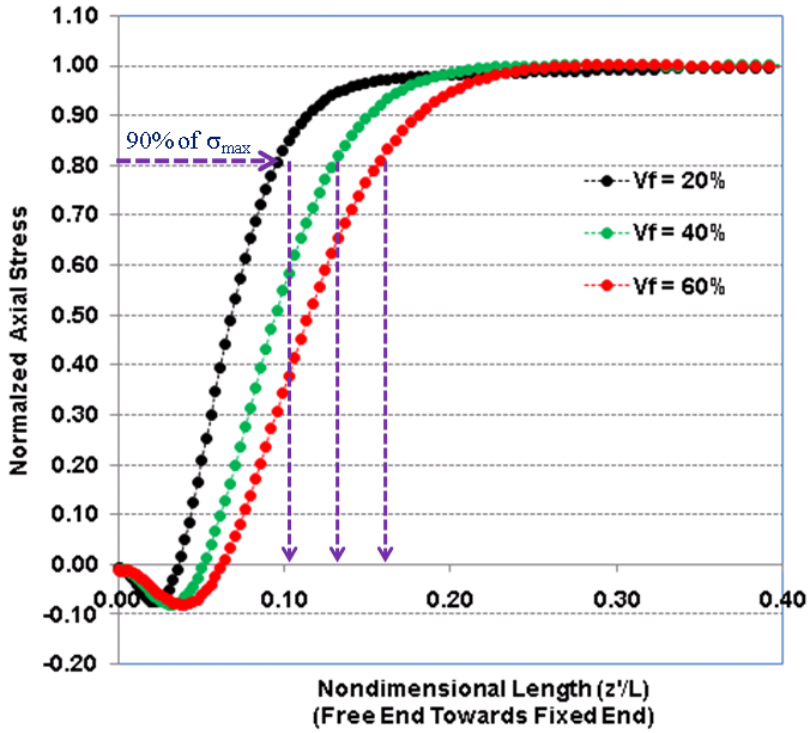

Figure 13. Comparison of ineffective fiber length with changing the fiber volume fraction. Axial stress was plotted along the fiber center (x = 0, y = 0 and z = 0 to L).

The UC-1 model was analyzed further to study the effect of matrix material on the stress distribution developed at the fiber-matrix interface. Stress distribution was compared when the matrix material was simulated using the mechanical properties of Polyethylene (PE) (E = 0.69 GPa = 0.69×10^{-3} N/μm^2, ν = 0.3) and Polyurethanes (PUR) (E = 1.3 GPa = 1.3×10^{-3} N/μm^2, ν = 0.3). In each case, Vectran properties (E = 75 GPa = 75×10^{-3} N/μm^2, ν = 0.3) were used for fiber material.

The axial and shear stress distributions at the fiber-matrix interface for the different matrix material is shown in Fig. 14. Near the free end, both axial and shear stresses were found to be reduced slightly for a relatively stronger matrix material PUR compared to PE. However, both stresses could be reduced further with additionally increasing the modulus of matrix material. For example, both the axial and shear stresses were found to be reduced significantly when the modulus of Vectran fiber was used to simulate the matrix material.

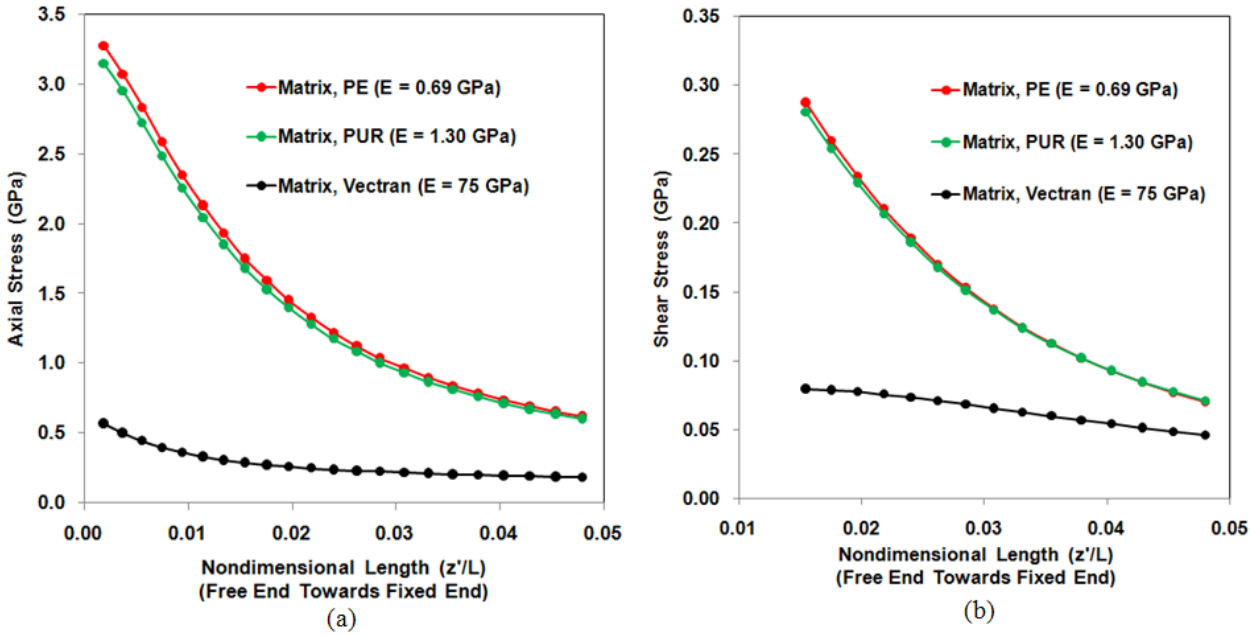

Figure 14. The effect of matrix material on (a) axial and (b) shear stress distribution at fiber-matrix interface.

The ineffective fiber length was found to be almost unaffected by changing the modulus of matrix material as shown in Fig. 15. It seems that the load transfer pattern from the matrix to fiber material is not significantly affected by the moduli ratio (E_f/E_m) of fiber and matrix materials.

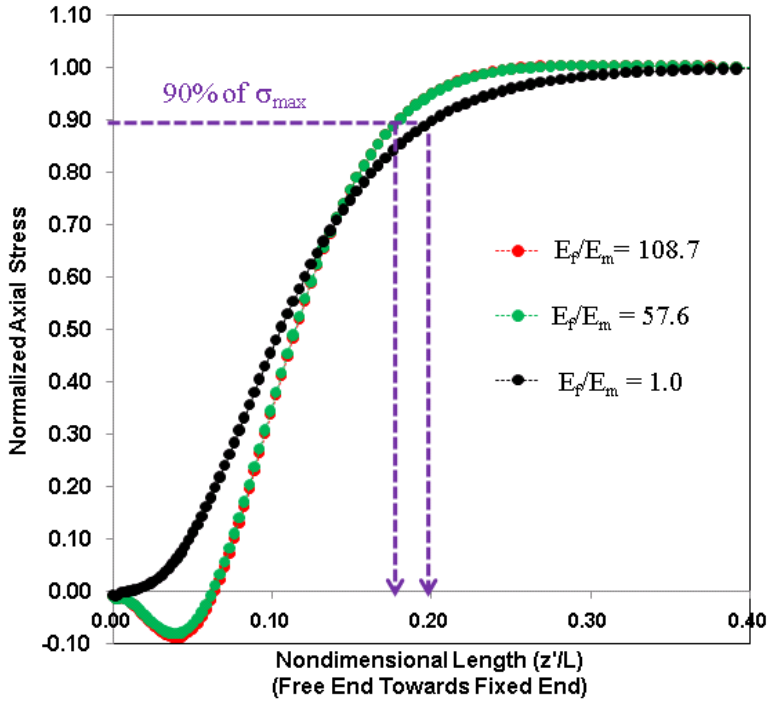

Figure 15. Comparison of ineffective fiber length with changing the matrix material. Axial stress was plotted along the fiber center (x = 0, y = 0 and z = 0 to L).

The bending simulation was then performed to investigate the effect of fiber scaling by comparing the stress distribution between the UC-1 and UC-2 models. First, the bending load was applied to the entire front surface covering both fiber and matrix regions; the load was applied such that the neutral axis remains at y = 0 plane. Since the bending load is not symmetric about the y = 0 plane, therefore full thickness (or depth, D) of the structure was modeled in simulation. For analysis convenience, only half of the volume of UC-1, as shown by shaded region in Figure 16, was modeled. Both unit cell models, UC-1 and UC-2, had the same length. Several displacement equations and contact analyses were used to enforce the required boundary conditions and loading as explained below.

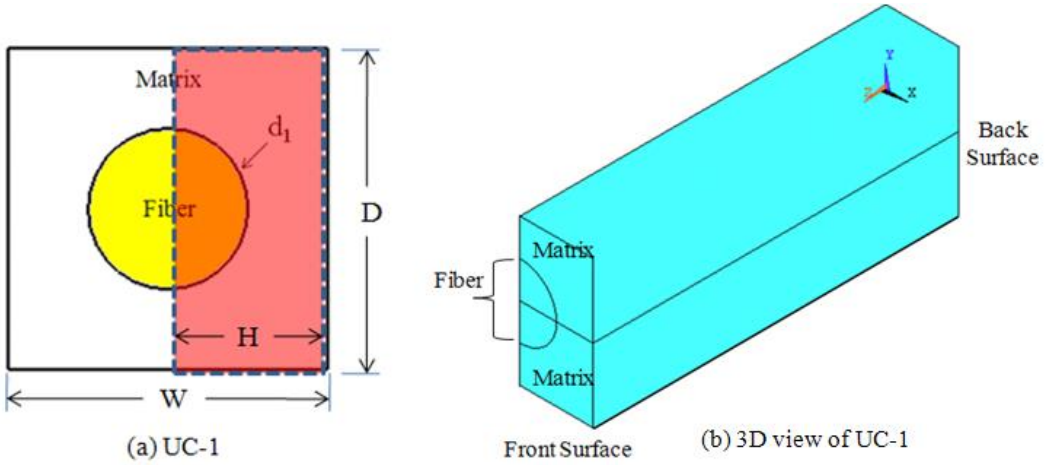

Figure 16. Minimum cross sectional area, shown by shaded region, required to model UC-1 in bending simulation.

At back surface (z = 0),

1) $u_3(x,y,0)$ for matrix nodes including fiber-matrix interface = 0
2) The nodes at the fiber region were used for simulating a contact analysis. It was needed under bending load since the upper portion of the broken fiber would tend to open while the lower portion would tend to close, and contacting each other. Therefore, a contact surface (slave) was created using the nodes located at the fiber region. And an analytical rigid surface (master) was created by using four corner nodes located at the back surface. The slave and master surfaces at z = 0 is shown in Figure 17 (a).

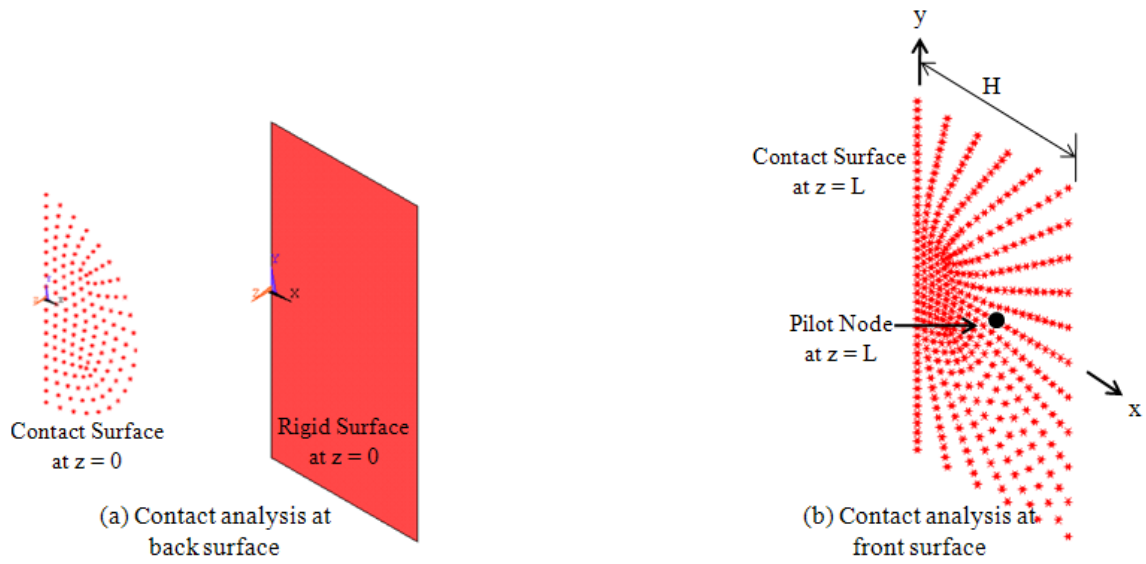

Figure 17. Slave and master surfaces used in bending simulation.

At front surface (z = L),

1) $u_3(x,0,L) = 0$, which represents zero z-displacement (u_3) of the centroidal axis. This enforces a pure bending condition and allows curvature and displacement along the model length only.
2) Another contact analysis was performed at front surface (z = L) to apply global bending load. First, a contact surface (slave) was created using nodes located at the entire front surface (z = L). Then, a master surface (pilot node) was created at (x = H/2, y = 0 and z = L). The bending moment, about the global x-axis (M_x), was applied at the pilot node, which ensured z-displacement, $u_3 = a*y$, where a = constant. The slave and master surfaces at z = L is shown in Figure 17 (b).

At the left and right surfaces, the following boundary conditions were applied to ensure global bending.

1) $u_1(0,y,z) = 0$
2) $u_1(H,y,z) = 0$, where H is the half width of the unit cell model along the global x-direction

At the top and bottom surfaces ($y = \pm D/2$), the free boundary conditions were applied.

Similar boundary conditions and contact analysis were also applied to UC-2 to simulate the bending load. The amount of bending moment (M_x) applied to pilot node of UC-1 was carefully chosen, which developed the maximum stress equal to the ultimate fiber strength. The total reaction force (absolute value) developed at the back surface was also recorded.

For a fair comparison between the unit cell models having the *same* cross-sectional area, the bending moment (M_x) applied to the pilot node was tuned to get the *same* reaction force (absolute value) at the back fixed surface. Under this loading situation, the z-displacement (u_3) of a particular node set is compared between the UC-1 and UC-2 models. For both models, the node set is located along the depth direction at (x = 0, y = -D/2 to D/2, and z = L). The comparison of z-displacement between the UC-1 and UC-2 models is shown in Figure 18 (a). The z-displacement is also compared for the *same bending moment* (M_x) applied to UC-1 and UC-2 models, and shown in Figure 18 (b). Both displacement profiles were found intuitively correct. However, the redistribution of fiber material as shown in Figure 18 (c) makes the UC-2 model a stiffer structure. Therefore, the UC-2 model, consisting of reduced fiber diameter, was found to offer reduced displacement compared to UC-1.

For the same node set, as mentioned earlier, the axial stress (σ_z) is also compared between the UC-1 and UC-2 models, and shown in Figure 19. The axial stress distribution along the depth direction was also found intuitively correct. The maximum axial stress at any depth (y-) dimension was found to be lower at UC-2, compared to that of UC-1.

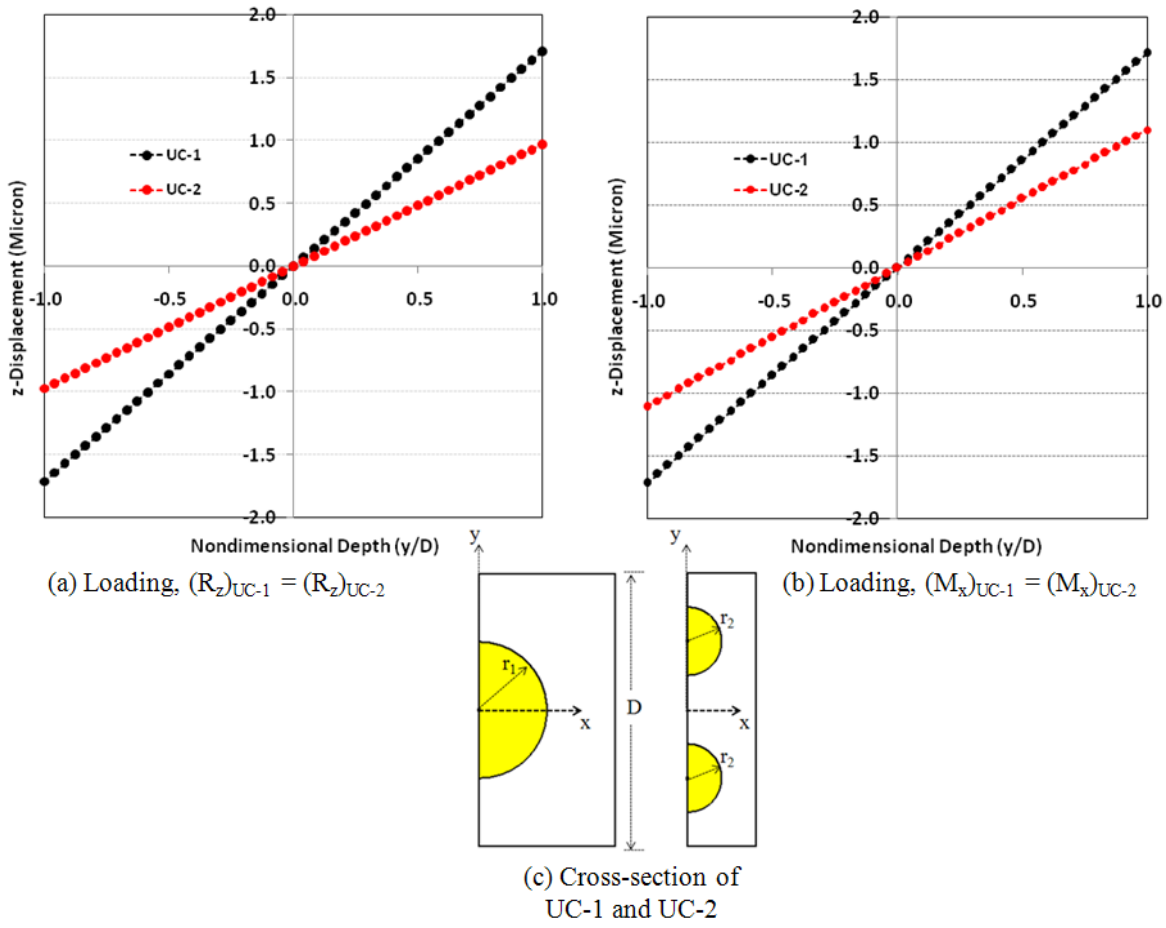

Figure 18: Comparison of z-displacement (u_z) between UC-1 and UC-2. Displacement is plotted for a node set located at the front surface (x = 0, y = -D/2 to D/2, and z = L).

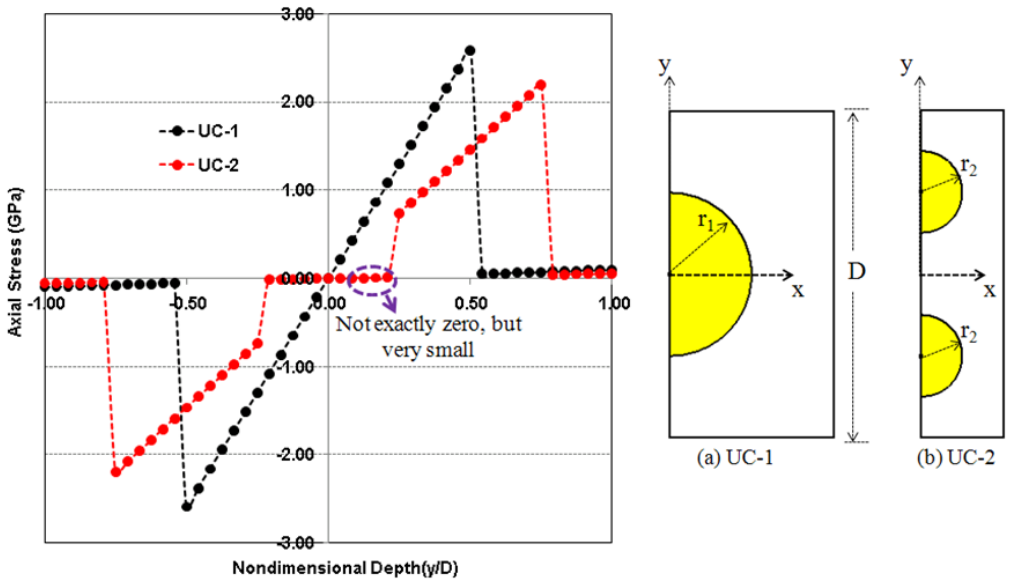

Figure 19: Comparison of axial stress (σ_z) between UC-1 and UC-2 along depth direction. Stress is plotted for a node set located at the front surface (x = 0, y = -D/2 to D/2, and z = L).

Finally, the axial stress of UC-1 and UC-2 is compared along the length (z-) direction and shown in Figure 20. In Figure 20(a), the axial stress is compared along a node path located at the fiber-matrix interface, which has different radial (or y-) dimension wrt the neutral axis for UC-1 and UC-2. In UC-1, the interface is located at radial dimension of 2.5 micron, whereas it is located at 3.75 micron wrt the neutral axis for UC-2. In Figure 20(b), the stress is plotted at the same radial dimension, 2.5 micron wrt neutral axis, for UC-1 and UC-2. However in all cases, the UC-2 with reduced fiber diameter was found to offer reduced axial stress compared to the UC-1.

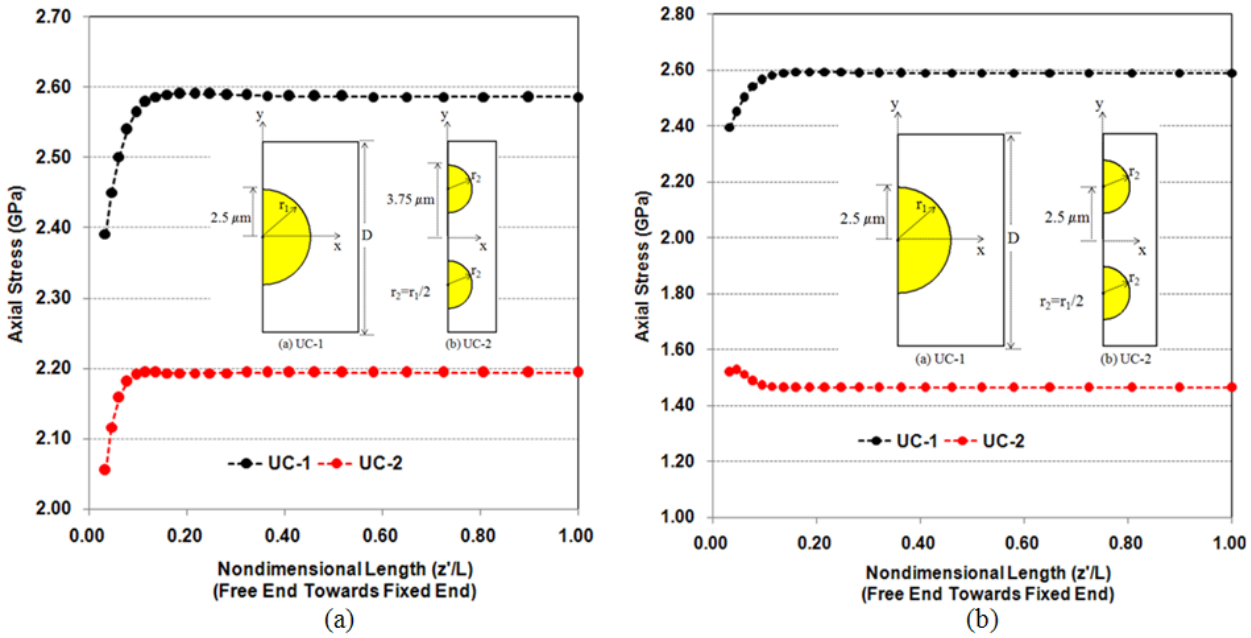

Figure 20: Comparison of axial stress (σ_z) between UC-1 and UC-2 along length direction. Stress is plotted for a node set located at (a) fiber-matrix interface, (b) same radial dimension (r = 2.5 micron) wrt neutral axis.

The axial stress distribution along the fiber-matrix interface is also studied to compare the ineffective fiber length, as defined earlier. The UC-2 was also found to offer slightly shorter ineffective fiber length compared to UC-1, as shown in Figure 21.

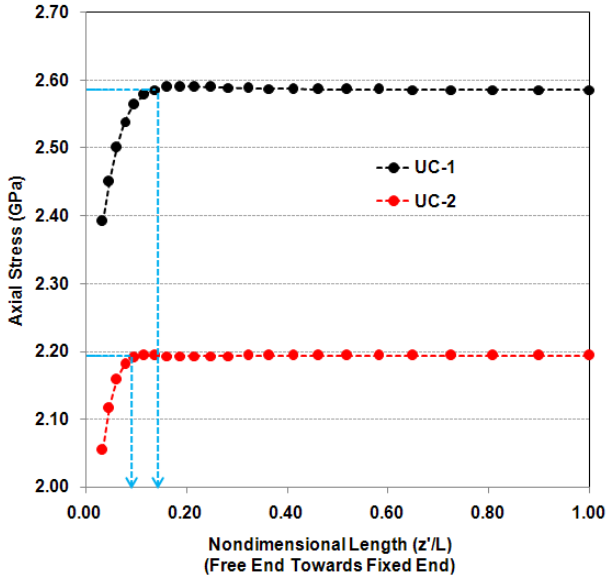

Figure 21: Comparison of ineffective fiber length between UC-1 and UC-2 under bending load.

No shear stress was developed at the fiber-matrix interface under the pure bending analysis. Therefore, the contact analysis performed at the front surface (z = L) of UC-1 and UC-2 was modified to develop noticeable shear stress at the fiber-matrix interface. In this case, the contact (or slave) surface was created using only the matrix nodes as shown in Figure 22 (b). The bending moment, about the global x-axis (M_x), was applied at the pilot node located at (x = H/2, y = 0, and z = L). As previously discussed, the back surface has contact boundary conditions as shown in Figure 22 (a).

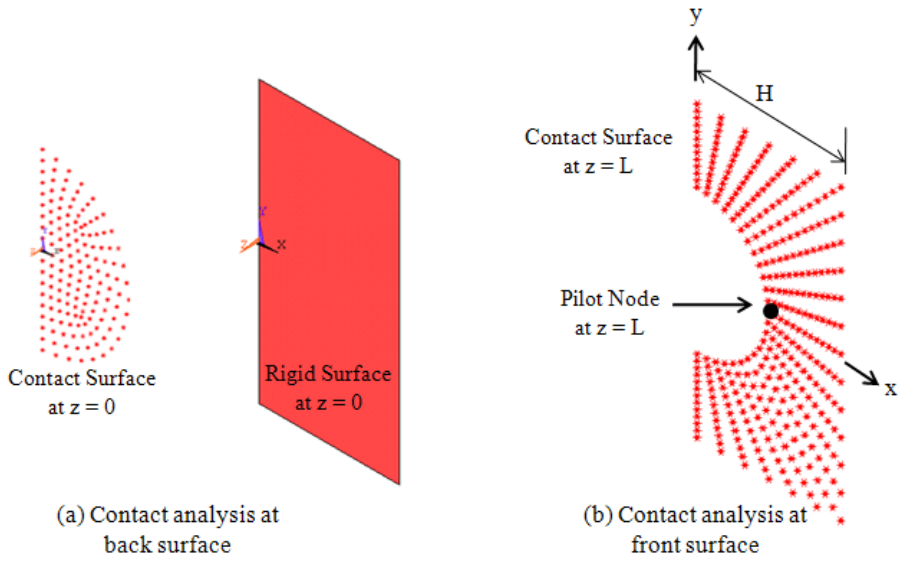

Figure 22. Slave and master surfaces used in bending simulation to develop noticeable shear stress at fiber-matrix interface.

The axial stress distribution along the fiber-matrix interface at the UC-1 and UC-2 is shown in Figure 23 (a). The axial stress was monitored at radial dimension of 2.5 μm and 3.75 μm wrt the centroidal axis for UC-1 and UC-2, respectively, as shown in Figure 23 (b). The UC-2 with smaller fiber diameter was found to offer reduced axial stress at higher radial dimension compared to the UC-1. As expected, the amount of axial stress reduction was found to be higher when the axial stress was compared at the same radial dimension (at 2.5 μm) for UC-1 and UC-2, as shown in Figure 24.

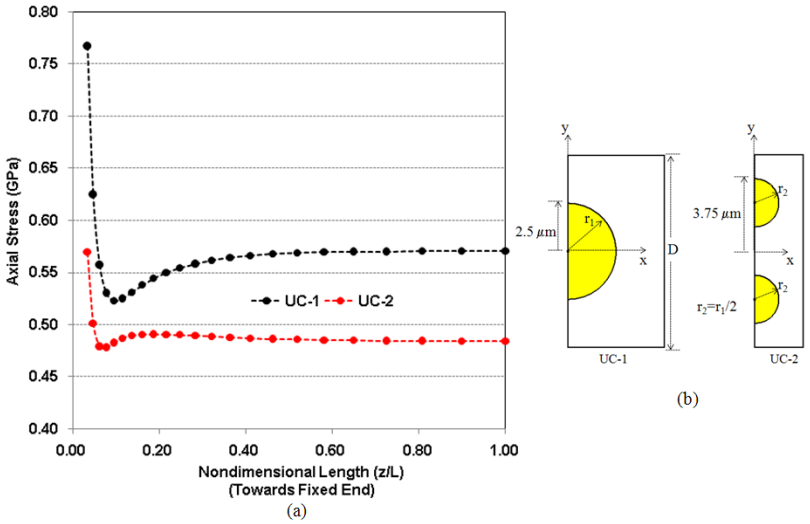

Figure 23: Comparison of axial stress (σ_z) between UC-1 and UC-2 along length direction at fiber-matrix interface.

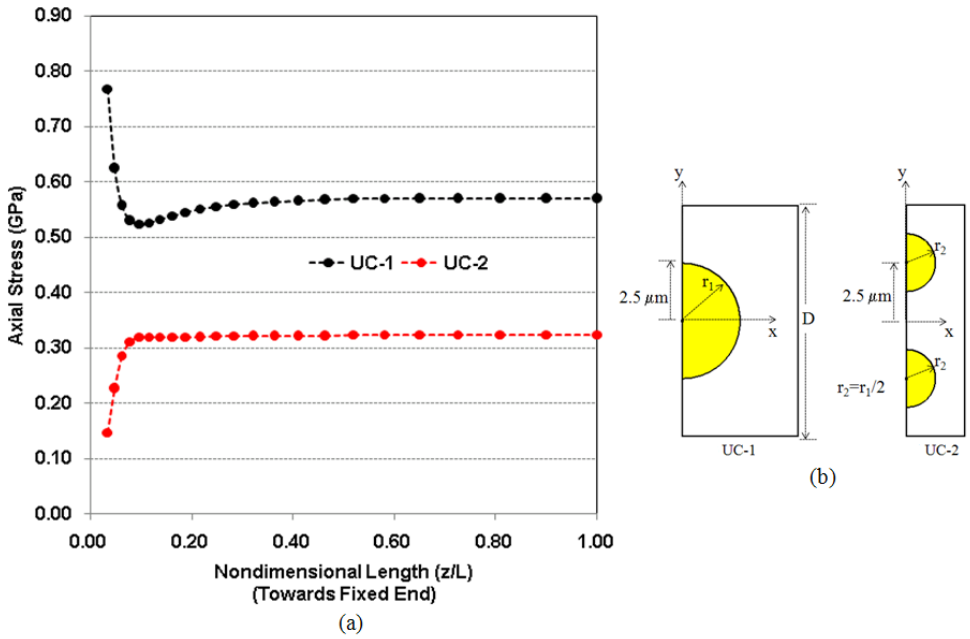

Figure 24: Comparison of axial stress (σ_z) between UC-1 and UC-2 along length direction at radial dimension of 2.5 micron.

The shear stress distributiondeveloped at the fiber-matrix interfaceis also compared between the UC-1 and UC-2 models. The stress was monitored at different radial dimension wrt the neutral axis for UC-1 and UC-2, as shown earlier in Figure 23(b). The shear stress in UC-2 was found to be reduced significantly compared to the UC-1, as shown in Figure 25.

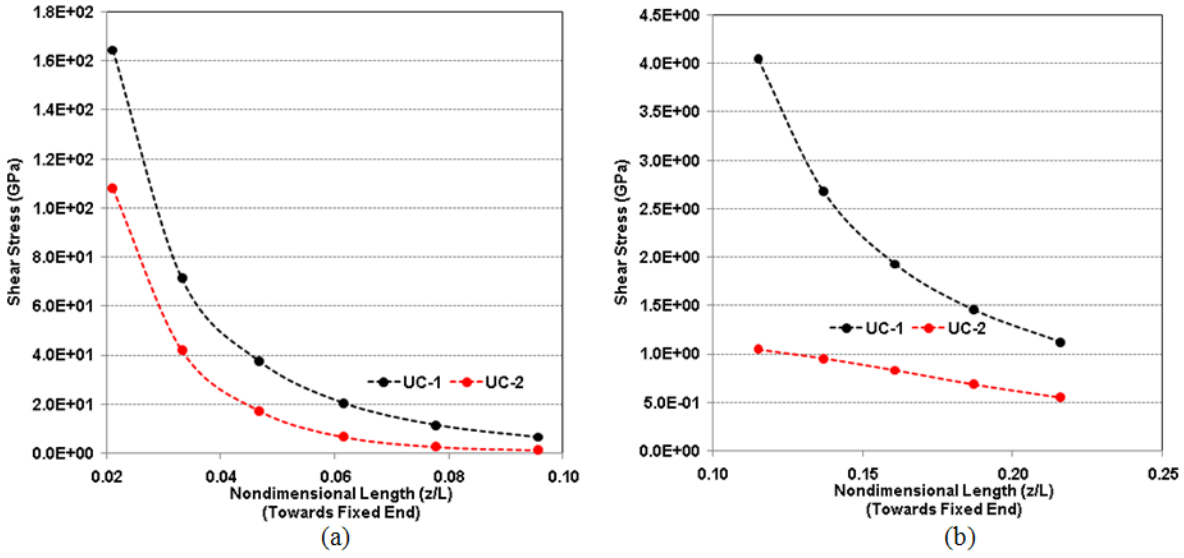

Figure 25: Comparison of shear stress between UC-1 and UC-2 models under bending load.

IV. Conclusion

This research pursued the possible advantages of using nanofibers (e.g., fibers with reduced diameter) instead of conventional fibers to improve the strength of flexible composites. The effect of fiber scaling was studied by numerical analysis of several unit cell models. It was shown in Figs. 2 and 4 that composite model consists of fibers with reduced diameter contains significantly more fiber surface area compared to the conventional composite at the same fiber volume fraction. Several unit cell models were developed and analyzed under the tensile and bending loads where the surface area of fiber was increased gradually, keeping the fiber volume fraction constant.

For each unit cell model, the standard values of vectran and polyethylene were used to mimic the fiber and matrix materials, respectively. First, the tensile simulation was performed where the axial and shear stresses developed at the fiber region (fiber center and fiber-matrix interface) were studied. The numerical analyses demonstrated that the ineffective fiber length, where the axial stress is less than 90% of its maximum value, was found to be improved in the unit cell models with reduced fiber diameter as shown in Fig. 9. The shear stress developed in the fiber-matrix interface was also found to be reduced significantly in the unit cell models with reduced fiber diameter as shown in Fig. 10. As composite model with reduced fiber diameter offers extensively more surface area compared to the conventional fiber model, the reduction in the shear stress was expected.

The unit cell model was then analyzed for different parametric analysis under tensile simulation. First, the effect of fiber volume fraction was examined. The axial stress, along the fiber center and fiber-matrix interface, was found to be reduced in proportion by increasing the fiber volume fraction as expected, and shown in Fig. 11. Similar result was obtained for shear stress distribution as shown in Fig. 12. However, the composite model with the minimum fiber volume fraction offered the shortest ineffective fiber length, or transferred the load from matrix to fiber within shortest distance, as shown in Fig. 13. The unit cell model was then analyzed further to study the effect of matrix material on the stress distribution developed at the fiber-matrix interface. Both axial and shear stresses, near the free end, were found to be reduced slightly for a relatively stronger matrix material. The stresses could be reduced further with additionally increasing the modulus of matrix material as shown in Fig. 14. However, the ineffective fiber length was found to be almost unaffected by changing the modulus of matrix material as shown in Fig. 15.

The unit cell models were then used for bending simulation. First, the bending load was applied globally to the entire front surface, i.e., matrix and fiber regions, using slave and master contact surfaces. Then, bending load was applied only to the matrix region to develop a noticeable shear stress at the fiber-matrix interface. In all situations, the unit cell models with reduced fiber diameter was found to be stiffer compared to the conventional fiber model, and subsequently offered reduced displacement (u_z) as shown in Fig. 18. The axial stress was then compared between the unit cell models. The stress was compared along the depth and length directions. In both cases, the unit cell model with reduced fiber diameter offered reduced axial stress compared to the conventional fiber model. These results are shown in Figs. 19 and 20. Similar results were found when the bending load was applied to the matrix region only as shown in Figs. 23 and 24. The ineffective fiber length under bending load was also found to be reduced with reducing the fiber diameter as shown in Fig. 21. Under bending load, the shear stress developed at the fiber-matrix interface also reduced significantly for reduced fiber model compared to the conventional composite as shown in Fig. 25.

In conclusion, this research demonstrated that composite model with reduced fiber diameter offers significantly more fiber surface area while keeping the fiber volume fraction constant. The increased surface area can help to minimize the ineffective fiber length, which, e.g., compensate for the imperfect bonding at the fiber-matrix interface. The reduced ineffective fiber length is also desirable to quickly transfer the load from matrix to fiber material. Composite model with reduced fibers also offered reduced shear stress developed in the fiber-matrix interface both in tensile and bending load situations. Therefore, composite materials consists of fiber with reduced diameter are expected to offer higher strength than a conventional composite prepared with the same volume fraction.

Acknowledgments

The faculty research grants for research and creative works offered from Eastern Washington University is acknowledged.

References

[1]Aboudi, J., "Micromechanical Analysis of Composites by the Method of Cells," ASME, 1989.
[2]Aboudi, J., "Micromechanics Prediction of Fatigue Failure of Composite Materials," Journal of Reinforced Plastic Composites, 1989.
[3]Goh, K.L., Aspden, R.M., Hukins, D.W.L., Shear lag models for stress transfer from an elastic matrix to a fiber in a composite material, *Int. J. Materials and Structural Integrity*, Vol. I, Nos. 1/2/3, 2007.
[4]Chon, C. T., & Sun, C. (1980). Stress distributions along a short fiber in fiber reinforced plastics. 15, 931-938.
[5]Xia, Z., Okabe, T., & Curtin, W. (2002). Shear-lag versus finite element models for stress transfer in fiber reinforced composites. 62, 1141-1149.
[6]Milliren, E.C., Nanocomposites: A Study of Theoretical Micromechanical Behavior Using Finite Element Analysis, *Graduate Thesis, Department of Mechanical and Industrial Engineering, Montana State University, Bozeman, Montana59717.*
[7]Hossain, N.M., Milliren, E.C., Woo, K. and Jenkins, C.H. (2010), "The Effect of Fiber Diameter on the Strength of Lightweight Composites," *51st AIAA/ASME/ASCE/AHS Structures, Structural Dynamics, and Material Conference*, Orlando, Florida.